

V1006 Cygni: Dwarf Nova Showing Three Types of Outbursts and Simulating Some Features of the WZ Sge-Type Behavior

Taichi KATO,^{1*} Elena P. PAVLENKO,² Alisa V. SHCHUROVA,³
Aleksii A. SOSNOVSKIY,² Julia V. BABINA,² Aleksii V. BAKLANOV,²
Sergey Yu. SHUGAROV,^{4,5} Colin LITTLEFIELD,⁶ Pavol A. DUBOVSKY,⁷
Igor KUDZEJ,⁷ Roger D. PICKARD,^{8,9} Keisuke ISOGAI,¹ Mariko KIMURA,¹
Enrique de MIGUEL,^{10,11} Tamás TORDAI,¹² Drahomir CHOCHOL,⁵
Yutaka MAEDA,¹³ Lewis M. COOK,¹⁴ Ian MILLER,¹⁵ Hiroshi ITOH,¹⁶

¹ Department of Astronomy, Kyoto University, Kyoto 606-8502, Japan

² Crimean Astrophysical Observatory, p/o Nauchny, 298409, Republic of Crimea

³ Taras Shevchenko National University of Kyiv, Glushkova ave., 4, 03127, Kyiv, Ukraine

⁴ Sternberg Astronomical Institute, Lomonosov Moscow State University, Universitetsky Ave., 13, Moscow 119992, Russia

⁵ Astronomical Institute of the Slovak Academy of Sciences, 05960, Tatranska Lomnica, the Slovak Republic

⁶ Department of Physics, University of Notre Dame, 225 Nieuwland Science Hall, Notre Dame, Indiana 46556, USA

⁷ Vihorlat Observatory, Mierova 4, 06601 Humenne, Slovakia

⁸ The British Astronomical Association, Variable Star Section (BAA VSS), Burlington House, Piccadilly, London, W1J 0DU, UK

⁹ 3 The Birches, Shobdon, Leominster, Herefordshire, HR6 9NG, UK

¹⁰ Departamento de Física Aplicada, Facultad de Ciencias Experimentales, Universidad de Huelva, 21071 Huelva, Spain

¹¹ Center for Backyard Astrophysics, Observatorio del CIECEM, Parque Dunar, Matalascañas, 21760 Almonte, Huelva, Spain

¹² Polaris Observatory, Hungarian Astronomical Association, Laborc utca 2/c, 1037 Budapest, Hungary

¹³ Kaminishiyamamachi 12-14, Nagasaki, Nagasaki 850-0006, Japan

¹⁴ Center for Backyard Astrophysics Concord, 1730 Helix Ct. Concord, California 94518, USA

¹⁵ Furzehill House, Ilston, Swansea, SA2 7LE, UK

¹⁶ Variable Star Observers League in Japan (VSOLJ), 1001-105 Nishiterakata, Hachioji, Tokyo 192-0153, Japan

*E-mail: *tkato@kusastro.kyoto-u.ac.jp

Received 201 0; Accepted 201 0

Abstract

We observed the 2015 July–August long outburst of V1006 Cyg and established this object to be an SU UMa-type dwarf nova in the period gap. Our observations have confirmed that V1006 Cyg is the second established object showing three types of outbursts (normal, long normal and superoutbursts) after TU Men. We have succeeded in recording the growing stage

of superhumps (stage A superhumps) and obtained a mass ratio of 0.26–0.33, which is close to the stability limit of tidal instability. This identification of stage A superhumps demonstrated that superhumps indeed slowly grow in systems near the stability limit, the idea first introduced by Kato et al. (2014). The superoutburst showed a temporary dip followed by a rebrightening. The moment of the dip coincided with the stage transition of superhumps, and we suggest that stage C superhumps is related to the start of the cooling wave in the accretion disk. We interpret that the tidal instability was not strong enough to maintain the disk in the hot state when the cooling wave started. We propose that the properties commonly seen in the extreme ends of mass ratios (WZ Sge-type objects and long-period systems) can be understood as a result of weak tidal effect.

Key words: accretion, accretion disks — stars: novae, cataclysmic variables — stars: dwarf novae — stars: individual (V1006 Cygni)

1 Introduction

Cataclysmic variables (CVs) are composed of a white dwarf and a red (or brown) dwarf supplying matter to the white dwarf, forming an accretion disk. Dwarf novae are a class of CVs characterized by outbursts. SU UMa-type dwarf novae are a subclass of dwarf novae which show superoutbursts in addition to normal outbursts. During superoutbursts, superhumps having periods a few percent longer than the orbital periods (P_{orb}) are observed and are considered to be the defining characteristics of SU UMa-type dwarf novae [For general information of CVs, SU UMa-type dwarf novae and superhumps, see e.g. Warner (1995a)]. The origin of superhumps and superoutbursts is currently understood as the consequence of the 3:1 resonance in the accretion disk resulting tidal instability combined with thermal instability (thermal-tidal instability model; Osaki 1989; Osaki, Kato 2013a). Only systems having mass ratios ($q = M_2/M_1$) smaller than ~ 0.3 can hold the radius of the 3:1 resonance inside the tidal truncation radius (Whitehurst 1988; Smith et al. 2007) and the appearance of superhumps in these systems gave a support to the tidal instability model for superhumps.

In recent years, it has been established that superhump periods during superoutbursts show systematic variations. Kato et al. (2009) showed that the evolution of superhumps has three stages: stage A (long, constant superhump period), stage B (short superhump period with systematic period variations) and stage C (constant period shorter than those of stage B superhump typically by 0.5%; seen in the late phase of the superoutburst to the post-superoutburst phase). Stage A superhumps are now considered to be superhumps during which the 3:1 resonance is growing and transition to stage B is considered to be caused by the pressure effect which produces a retrograde precession (Osaki, Kato 2013b; Kato, Osaki 2013). The origin of stage C superhumps is still unknown. It has been well established that period variations during stage B are a good function of P_{orb} for systems with short P_{orb} (cf. Kato et al. 2009; Kato et al. 2015). In long- P_{orb} systems, however, there

have been a number of objects showing a strong decrease of the superhump periods [the best-known examples are MN Dra and UV Gem, see subsection 4.10 in Kato et al. (2009)]. The origin of strongly negative period derivatives had remained a mystery. Kato et al. (2014) proposed a working hypothesis that what looked like strongly negative period derivatives for stage B superhumps in such systems are actually caused by stage A-B transition based on the photometrically detected P_{orb} in MN Dra. Kato et al. (2014) suggested that the 3:1 resonance grows slower in systems having large q close to the stability border of the resonance and that this is observed as long-lasting stage A. This interpretation violated the received wisdom that long-lasting stage A reflects the small q , as is typically seen in WZ Sge-type dwarf novae (Kato 2015), which have completely opposite properties to long-orbital systems. Since the discussion in Kato et al. (2014) was based on the yet unconfirmed P_{orb} of MN Dra, further confirmation is clearly needed. We present the detection of long-lasting growing superhumps in a long- P_{orb} system V1006 Cyg having a spectroscopically established P_{orb} .

V1006 Cyg was discovered as a dwarf nova (S 7844) (Hoffmeister 1963a; Hoffmeister 1963b) with a photographic range of 16–18 mag. Gessner (1966) derived an outburst cycle length of 13.5 d. Bruch et al. (1987) recorded another outburst. Bruch, Schimpke (1992) obtained a spectrum and established this object to be a dwarf nova. Due to the initially reported faintness, this object had not been well studied since then. Since 2005, AAVSO observers started regular monitoring using CCDs and recorded an outburst reaching $V=13.6$ on 2006 June 24. This outburst lasted at least for 4 d. Sheets et al. (2007) performed a radial-velocity study and obtained P_{orb} of 0.09903(9) d. Since this period places the object in the period gap, the slowly fading 2006 outburst was suspected to be a superoutburst. Upon a bright (unfiltered CCD magnitude 13.6) outburst on 2007 August 14, a search for superhumps was conducted (vsnet-alert 9471). Although short-term modulations were detected, these variations were later found to be orbital

variations (vsnet-alert 9489). This observation and the observation of a similar bright outburst in 2009 September (vsnet-alert 11490, 11508) were examined in detail by Pavlenko et al. (2014) and the absence of superhumps was confirmed.

On 2015 July 12, ASAS-SN (Shappee et al. 2014; Danilet et al. in preparation) detected an outburst at $V=14.1$ (vsnet-alert 18846). This outburst was detected sufficiently early and the initial phase of the outburst was observed. The object reached $V=13.6$ and low-amplitude superhumps were detected on July 15–16 (vsnet-alert 18851). The superhumps were observed to glow until July 18 (BJD 2457222) (see figure 1).

2 Observation and Analysis

The data were obtained under campaigns led by the VSNET Collaboration (Kato et al. 2004). We also used the public data from the AAVSO International Database¹. Time-resolved observations were performed in 13 different locations by using 30cm-class telescopes (table 2). We deal with observations until August 7. The data analysis was performed just in the same way described in Kato et al. (2009) and Kato et al. (2014) and we mainly used R software² for data analysis. In de-trending the data, we divided the data into four segments in relation to the outburst phase and used locally-weighted polynomial regression (LOWESS: Cleveland 1979) except the rising segment of a rebrightening. During the rising phase of the rebrightening a third order polynomial fitting was instead used. The times of superhumps maxima were determined by the template fitting method as described in Kato et al. (2009). The times of all observations are expressed in barycentric Julian Days (BJD).

3 Discussion

3.1 Identification of superhump stages

The amplitudes of superhumps before BJD 2457220 were small, indicating that we recorded the growing stage (stage A) of superhumps. Although the observations before BJD 2457220 were short and the initial night suffered from poor conditions, observations between BJD 2457221 and 2457223 were of sufficient quality to determine the period in the early phase (table 3). The $O-C$ analysis ($17 \leq E \leq 28$) and PDM analysis yielded periods of 0.1073(2) d and 0.1076(1) d, respectively. The period of 0.1075 d (average of the two methods) is 8.5% longer than P_{orb} , giving an exceptionally large fractional superhump excess. Since the amplitudes of superhumps on BJD 2457221 already approached the maximum, these periods are likely shorter than the true period of stage A superhumps, because the pressure effect starts to dominate when superhumps fully grow and

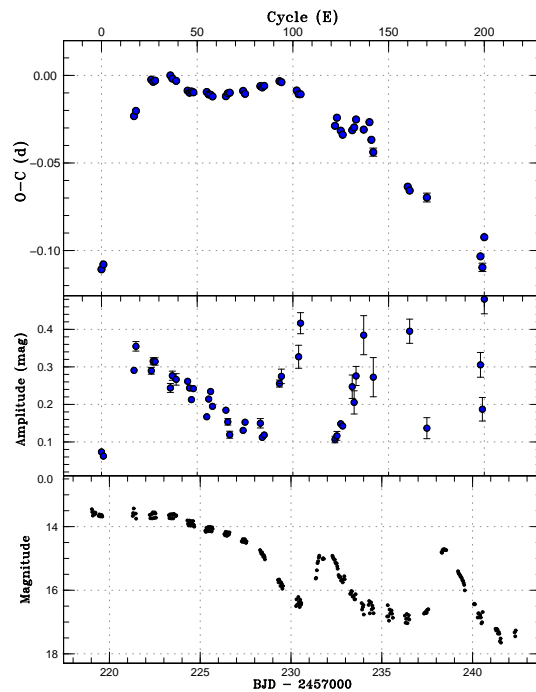


Fig. 1. $O-C$ diagram of superhumps in V1006 Cyg (2015). (Upper:) $O-C$ diagram. We used a period of 0.10541 d for calculating the $O-C$ residuals. The superhump maxima up to $E = 28$ are stage A superhumps, maxima between $E=36$ and $E = 94$ have a positive period derivative and are identified as stage B superhumps. After this, the period decreased to a constant one (stage C superhumps). (Middle:) Amplitudes of superhumps. The amplitudes were small around $E = 0$. The $O-C$ diagram suggests that stage A-B transition occurred somewhere between $E = 28$ and $E = 36$. The superhump amplitudes monotonously decreased during the superoutburst. After $E = 100$, the amplitudes became large (0.3–0.4 mag) when the object faded. (Lower:) Light curve. The data were binned to 0.035 d. The initial outburst detection was on BJD 2457215.9, 3 d before the start of our observation. It took 6 d for this object to fully develop stage B superhumps. The maximum on BJD 2457232 is a rebrightening. The maximum on BJD 2457238 is the first normal outburst of regular series of outbursts following a superoutburst.

reduces the precession rate (Kato, Osaki 2013). By using this period as an approximate period of stage A superhumps and with the strong expectation that the true period of stage A superhumps is longer than this period, we have been able to resolve the ambiguity in the cycle counts between BJD 2457220 and 2457221. The cycle counts in table E2 are based on this identification. The resultant mean period of stage A superhumps between BJD 2457219 and 2457223 by the $O-C$ analysis is 0.1093(3) d, which we consider the best period from the present observations. This period gives ϵ^* of 0.094(3), which correspond to $q=0.34(2)$.

The duration of stage A was at least 32 cycles. Although the true duration of the growing phase of superhumps is unknown in this object due to the observational gap, the close similarity of the $O-C$ diagram and variation of superhumps amplitudes between V1006 Cyg and MN Dra (figure 2) suggests it took long time to develop superhumps in this system. It also took 6 d (~ 60

¹ <<http://www.aavso.org/data-download>>.

² The R Foundation for Statistical Computing:
<<http://cran.r-project.org/>>.

cycles) since the outburst detection to fully develop stage B superhumps based on the $O-C$ diagram. Since this object has relatively frequent outbursts, it is likely that the Case A outburst of Osaki, Meyer (2003) classification should occur in this object. However, the observed delay in superhumps likely reflects the long growth time of superhumps (just like the Case B outburst for low- q system; in most ordinary SU UMa-type dwarf novae, the growing stage of superhumps is rarely recorded a few days after the outburst detection, e.g. Kato et al. 2009). This delay of appearance of stage B superhumps is unusually long for an ordinary SU UMa-type dwarf nova and is even comparable to extreme WZ Sge-type objects (cf. Kato 2015).

After reaching the maximum amplitude, the superhump period became short as in stage B superhumps in ordinary SU UMa-type dwarf novae (Kato et al. 2009; Kato, Osaki 2013). We identified $40 \leq E \leq 98$ as stage B and obtained a mean period of 0.10541(4) d and a period derivative $P_{\text{dot}} = \dot{P}/P$ of $+20.8(2.0) \times 10^{-5}$. The $O-C$ analysis indicates that the times of superhumps for $E \geq 106$ can be very well expressed by a period of 0.10444(5) d, which we consider the period of stage C superhumps.

3.2 Mass ratio from stage A superhumps

As described in subsection 3.1, the modern method using stage A superhumps gives a very large mass ratio of $q=0.34(2)$. Since the early part of the observations was not ideally obtained, we give a firmly determined lower limit of the period of stage A superhumps (0.1075 d), which corresponds to $q \geq 0.26$. These lower limit is close to the borderline ($q=0.24$) of the development of superhumps in 3-D numerical simulation (Smith et al. 2007). Our best value is close to the limit $q \sim 0.33$ to develop the 3:1 resonance under condition of reduced mass-transfer (Murray et al. 2000). Although our observation suffered from uncertainty due to the gap in the observation, we have demonstrated that stage A superhump method is applicable to systems close to the stability limit.

3.3 Mass ratio and disk radius from stage C superhumps

As described in Kato, Osaki (2013), the precession rate of stage C superhumps can be used to estimate the disk radius if the mass ratio is known, since the pressure effect can be neglected in cool post-superoutburst disks. If the disk radius can be estimated, we can constrain the mass ratio (e.g. Kato et al. 2013b). The measured ϵ^* for stage C superhumps of V1006 Cyg is 0.0518(10). This value corresponds to a disk radius of $0.37A$, where A is the binary separation, for $q=0.26$ and $0.34A$ for $q=0.34$.

3.4 Stage B-C transition and rebrightening

The stage B-C transition described in subsection 3.1 occurred during the rapid decline from the superoutburst plateau. This feature is different from the behavior from the one in “textbook” SU UMa-type dwarf novae, in which stage B-C transition usually occurs during the later part of the superoutburst plateau and is usually associated with a small brightening trend (Kato et al. 2009). In V1006 Cyg, the object instead faded and a rebrightening was recorded after the transition. Six days after this rebrightening, the object underwent another outburst. As judged from the subsequent behavior (E. Pavlenko et al. in preparation), this outburst was the first normal outburst of the regular cycle of normal outbursts.³

The origin of stage B-C transition is still poorly understood. In the present case, it appears that the cooling front started before the termination of the plateau phase, since the first rebrightening occurred only three days after the rapid fading. Although such early occurrence of a rebrightening is rarely met in ordinary SU UMa-type dwarf novae, similar one was observed in the long- P_{orb} system MN Dra (see figure 3 in Antipin, Pavlenko 2002). We propose that the mass ratio close to the stability border of the 3:1 resonance in V1006 Cyg made it difficult to maintain the tidal instability, and the thermal and tidal instabilities decoupled as proposed for ER UMa-type objects and WZ Sge-type rebrightenings as suggested by Hellier (2001). Although Hellier (2001) considered that small q is responsible for this phenomenon, we can extend the same discussion to objects with large q close to the stability border of the 3:1 resonance.

It would be worth mentioning that stage B-C transition is not usually observed in WZ Sge-type objects (Kato 2015). It is possible that rapid fading from the superoutburst plateau (often seen as a temporary dip) in WZ Sge-type dwarf novae has the same properties as in V1006 Cyg. The common behavior (termination of the plateau phase before appearance of stage C superhumps, dip-like fading and rebrightening) in WZ Sge-type objects and objects having mass ratios close to the stability border may be understood in a unified way: the small effect of the small tidal torque is unable to maintain the hot state when the cooling front starts.

3.5 Comparison with TU Mensae

Up to this work, TU Men was the only established dwarf nova that shows three types of outbursts (normal, long normal and superoutbursts; the names here are given in modern sense) (Warner 1995b; Bateson et al. 2000). The only other possible example is NY Ser (Pavlenko et al. 2014) which showed outbursts with intermediate durations without superhumps. Since

³ The identification as a rebrightening is also based on the similarity of the behavior with the SU UMa-type dwarf nova QZ Ser in the period gap (T. Ohshima et al. in prep.), which shows only very infrequent outbursts.

there were outbursts in V1006 Cyg lasting more than six days (2007) and more than five days (2009) without superhumps (Pavlenko et al. 2014), the present detection of a genuine superoutburst makes V1006 Cyg the second case showing three types of outbursts. This indicates that P_{orb} above the period gap is not an essential condition for displaying such behavior.

3.6 Comparison with other systems

The interpretation that superhumps slowly grow in systems with mass ratios close to the stability limit was first presented in Kato et al. (2014) for MN Dra. Although there still remains uncertainty about P_{orb} of MN Dra, and the identification of superhumps stages remained somewhat unclear, the present detection of growing superhumps in V1006 Cyg has established this interpretation. In table 1, we list the objects having long orbital (or superhump) periods and long-lasting stage A superhumps. The suspected orbital periods for MN Dra and CRTS J214738.4+244554 are taken from Pavlenko et al. (2010) and Kato et al. (2013a), respectively. By using this period, we could also obtain the mass ratio for CRTS J214738.4+244554 from stage A superhumps. All the obtained mass ratios are in the range of 0.20–0.34, consistent with the theoretical stability limit.

Acknowledgments

This work was supported by the Grant-in-Aid “Initiative for High-Dimensional Data-Driven Science through Deepening of Sparse Modeling” (25120007) from the Ministry of Education, Culture, Sports, Science and Technology (MEXT) of Japan. This work also was partially supported by grants of RFBR 15-32-50920 and 15-02-06178, 14-02-00825 and by the VEGA grant No. 2/0002/13.

Supporting information

Additional supporting information can be found in the online version of this article: Figure 2, Tables 1, 2, 3.

Supplementary data is available at PASJ Journal online (*included at the end in this astro-ph version*).

References

- Antipin, S. V., & Pavlenko, E. P. 2002, A&A, 391, 565
 Bateson, F., McIntosh, R., & Stubbings, R. 2000, Publ. Variable Stars Sect. R. Astron. Soc. New Zealand, 24, 48
 Bruch, A., Fischer, F.-J., & Wilmsen, U. 1987, A&AS, 70, 481
 Bruch, A., & Schimpke, T. 1992, A&AS, 93, 419
 Cleveland, W. S. 1979, J. Amer. Statist. Assoc., 74, 829
 Gessner, H. 1966, Veröff. Sternw. Sonneberg, 7, 61
 Hellier, C. 2001, PASP, 113, 469
 Hoffmeister, C. 1963a, Mitteil. Veränderl. Sterne, 751
 Hoffmeister, C. 1963b, Astron. Nachr., 287, 169
 Kato, T. 2015, PASJ, 67, 108
 Kato, T., et al. 2014, PASJ, 66, 90
 Kato, T., et al. 2015, PASJ, 67, 105
 Kato, T., et al. 2013a, PASJ, 65, 23
 Kato, T., et al. 2009, PASJ, 61, S395
 Kato, T., Monard, B., Hamsch, F.-J., Kiyota, S., & Maehara, H. 2013b, PASJ, 65, L11
 Kato, T., & Osaki, Y. 2013, PASJ, 65, 115
 Kato, T., Uemura, M., Ishioka, R., Nogami, D., Kunjaya, C., Baba, H., & Yamaoka, H. 2004, PASJ, 56, S1
 Murray, J., Warner, B., & Wickramasinghe, D. 2000, New Astron. Rev., 44, 51
 Osaki, Y. 1989, PASJ, 41, 1005
 Osaki, Y., & Kato, T. 2013a, PASJ, 65, 50
 Osaki, Y., & Kato, T. 2013b, PASJ, 65, 95
 Osaki, Y., & Meyer, F. 2003, A&A, 401, 325
 Pavlenko, E. P., et al. 2014, PASJ, 66, 111
 Pavlenko, E. P., et al. 2010, Astron. Rep., 54, 6
 Shappee, B. J., et al. 2014, ApJ, 788, 48
 Sheets, H. A., Thorstensen, J. R., Peters, C. J., Kapusta, A. B., & Taylor, C. J. 2007, PASP, 119, 494
 Smith, A. J., Haswell, C. A., Murray, J. R., Truss, M. R., & Foulkes, S. B. 2007, MNRAS, 378, 785
 Warner, B. 1995a, Cataclysmic Variable Stars (Cambridge: Cambridge University Press)
 Warner, B. 1995b, Ap&SS, 226, 187
 Whitehurst, R. 1988, MNRAS, 232, 35

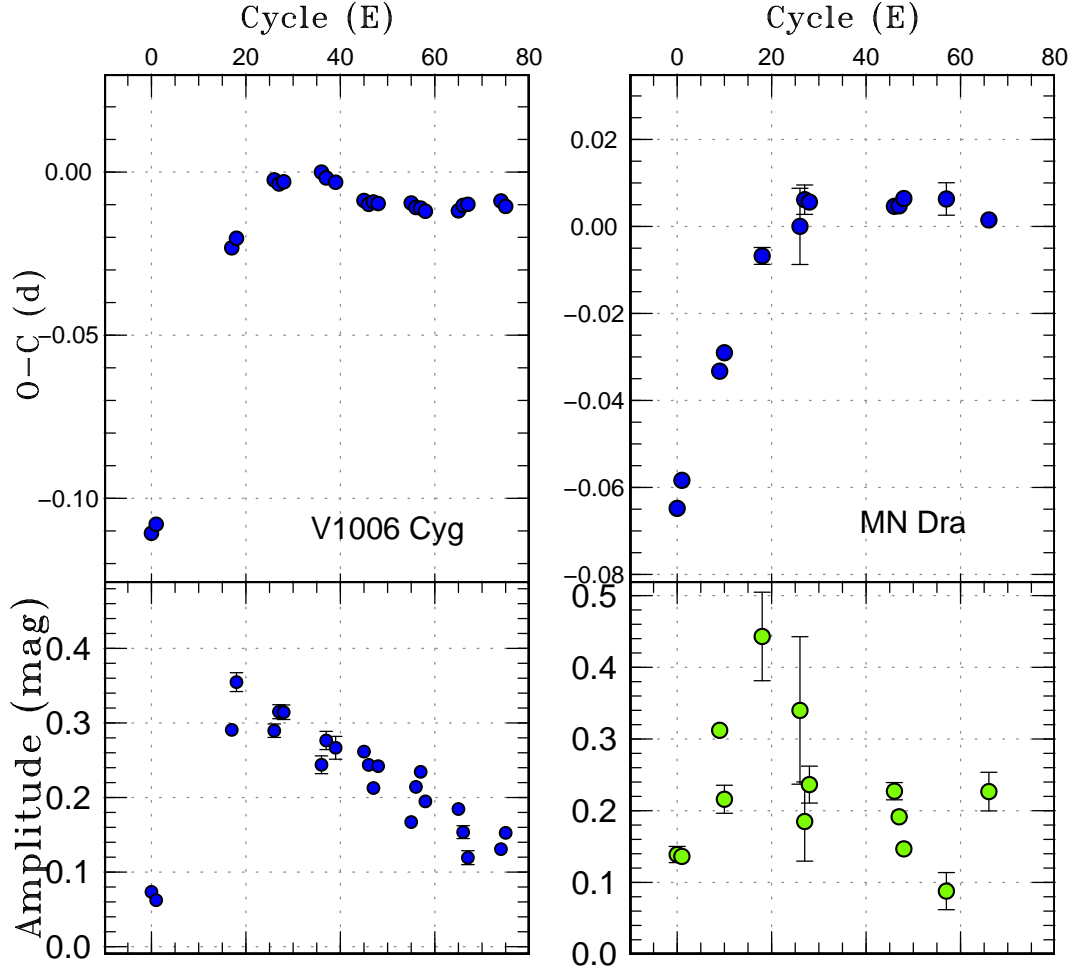


Fig. 2. Comparison of $O - C$ diagrams and variation of superhump amplitudes in V1006 Cyg and MN Dra. The data for MN Dra are taken from Kato et al. (2014). The behavior of $O - C$ diagrams are almost the same in both systems. In MN Dra with denser observations in the early part, the slow growth of the superhump amplitudes for two nights were recorded. Based on the similarity of the $O - C$ diagrams, we consider that the superhump amplitudes also grow slowly in V1006 Cyg.

Table 1. Comparison of SU UMA-type objects with long phase of stage A superhumps

Object	P_{orb}^*	P_A^\dagger	P_B^\ddagger	P_C^\S	dur $^\parallel$	$q^\#$	References
V1006 Cyg (2015)	0.09903(9)	0.1093(3)	0.10541(4)	0.10444(5)	≥ 32	0.34(2)	This work
MN Dra (2012)	0.0998(2)	0.10993(9)	0.10530(6)	–	≥ 39	0.327(5)	Kato et al. (2014)
MN Dra (2013)	0.0998(2)	0.1082(1)	0.10504(7)	–	≥ 18	0.258(5)	Kato et al. (2014)
CRTS J214738.4+244554 (2011)	0.09273(3)	0.0992(3)	0.09715(2)	–	≥ 21	0.204(11)	Kato et al. (2015)
OT J064833.4+065624 (2014)	–	0.1052(4)	0.10033(3)	–	≥ 38	–	Kato et al. (2015)

*Orbital period (d).

† Period of stage A superhumps (d).

‡ Period of stage B superhumps (d).

§ Period of stage C superhumps (d).

$^\parallel$ Duration of stage A (cycles).

$^\#$ Determined from stage A superhumps.

Table 2. Superhump maxima of V1006 Cyg (2015)

E	max*	error	$O - C^\dagger$	N^\ddagger
0	57219.4523	0.0008	-0.1077	156
1	57219.5605	0.0011	-0.1046	106
17	57221.3318	0.0001	-0.0155	288
18	57221.4401	0.0006	-0.0123	42
26	57222.3013	0.0004	0.0077	120
27	57222.4055	0.0004	0.0068	72
28	57222.5115	0.0004	0.0077	71
36	57223.3578	0.0007	0.0129	69
37	57223.4614	0.0006	0.0113	55
39	57223.6709	0.0006	0.0106	49
45	57224.2978	0.0004	0.0066	58
46	57224.4020	0.0003	0.0057	339
47	57224.5081	0.0003	0.0067	393
48	57224.6131	0.0004	0.0065	104
55	57225.3511	0.0005	0.0086	100
56	57225.4551	0.0004	0.0075	223
57	57225.5604	0.0004	0.0076	175
58	57225.6648	0.0006	0.0069	72
65	57226.4028	0.0004	0.0089	167
66	57226.5099	0.0008	0.0108	153
67	57226.6156	0.0013	0.0114	72
74	57227.3545	0.0008	0.0144	74
75	57227.4583	0.0007	0.0130	73
83	57228.3059	0.0009	0.0195	45
84	57228.4106	0.0007	0.0191	97
85	57228.5169	0.0008	0.0202	113
93	57229.3629	0.0005	0.0251	55
94	57229.4677	0.0010	0.0248	44
102	57230.3062	0.0011	0.0222	52
103	57230.4096	0.0012	0.0204	126
104	57230.5149	0.0010	0.0206	86
122	57232.3943	0.0010	0.0075	56
123	57232.5043	0.0014	0.0124	57
125	57232.7077	0.0006	0.0055	539
126	57232.8108	0.0006	0.0035	531
131	57233.3405	0.0018	0.0074	43
132	57233.4475	0.0018	0.0093	140
133	57233.5574	0.0017	0.0141	36
137	57233.9733	0.0019	0.0094	24
140	57234.2937	0.0009	0.0145	53
141	57234.3891	0.0010	0.0047	57
142	57234.4874	0.0023	-0.0021	57
160	57236.3651	0.0009	-0.0169	121
161	57236.4683	0.0011	-0.0188	109
170	57237.4130	0.0025	-0.0204	110
198	57240.3309	0.0015	-0.0464	87
199	57240.4300	0.0024	-0.0523	115
200	57240.5527	0.0014	-0.0349	69

*BJD-2400000.

†Against max = 2457219.5600 + 0.105138.

‡Number of points used to determine the maximum.

Table 3. Log of observations of V1006 Cyg (2015)

Start*	End*	N^\dagger	Code [‡]	filter [§]	Start*	End*	N^\dagger	Code [‡]	filter [§]
57219.0237	57219.2394	405	Mdy	V	57231.7318	57231.8181	484	LCO	C
57219.3980	57219.4864	67	Trt	C	57232.2778	57232.5673	196	CRI	V
57219.4226	57219.6117	249	RPc	V	57232.6069	57232.8478	1163	LCO	C
57221.2790	57221.3793	87	CRI	I	57232.7119	57232.9519	350	COO	C
57221.2793	57221.3796	87	CRI	R	57233.2564	57233.5640	195	CRI	V
57221.2796	57221.3787	86	CRI	B	57233.3993	57233.4743	94	RPc	V
57221.2799	57221.3790	85	CRI	V	57233.8786	57234.0075	39	COO	C
57221.4283	57221.4774	42	IMi	V	57234.2623	57234.5547	198	CRI	V
57222.2065	57222.2836	113	Ioh	C	57235.2832	57235.5584	183	CRI	V
57222.2594	57222.5643	280	CRI	V	57235.3232	57235.5705	165	DPV	C
57223.2543	57223.5649	292	CRI	V	57235.3672	57235.5476	124	Shu	C
57223.6402	57223.6791	49	deM	C	57235.4643	57235.6187	13	COO	C
57224.2714	57224.5465	230	CRI	V	57236.2541	57236.5254	125	CRI	V
57224.3371	57224.5392	260	DPV	C	57236.3156	57236.5207	177	Shu	C
57224.3705	57224.6742	359	deM	C	57237.3182	57237.5208	143	Shu	C
57224.4079	57224.5132	128	RPc	V	57237.3766	57237.5597	72	CRI	V
57224.4289	57224.5236	124	IMi	V	57238.2883	57238.5461	103	CRI	V
57225.2640	57225.5473	191	CRI	V	57238.3035	57238.3228	17	Shu	C
57225.3599	57225.4483	114	DPV	C	57238.3495	57238.5317	123	DPV	C
57225.4328	57225.6789	301	deM	C	57238.3909	57238.5692	180	RPc	C
57225.4685	57225.5695	113	Trt	V	57238.4168	57238.5540	192	Trt	V
57226.3121	57226.5320	276	DPV	C	57239.1894	57239.2957	279	KU1	C
57226.3679	57226.4597	73	CRI	V	57239.2470	57239.5708	178	CRI	V
57226.4991	57226.6241	174	RPc	V	57239.2983	57239.5495	79	Shu	V
57227.2796	57227.5517	240	CRI	V	57239.3176	57239.4514	98	Trt	V
57228.2790	57228.5579	186	CRI	V	57240.0578	57240.1351	193	KU1	C
57228.3883	57228.5653	118	DPV	C	57240.2694	57240.5664	201	CRI	V
57229.2688	57229.5634	181	CRI	V	57240.3250	57240.5372	144	DPV	C
57230.2753	57230.5615	127	CRI	V	57241.2502	57241.5681	214	CRI	V
57230.3108	57230.5230	144	DPV	C	57241.3033	57241.3973	65	DPV	C
57230.3801	57230.4999	58	Trt	V	57241.3375	57241.4990	43	Kaz	C
57231.3481	57231.5638	100	CRI	V	57242.2957	57242.3778	56	DPV	C

*JD–2400000.

[†]Number of observations.[‡]Key to observers: COO (L. Cook), CRI (Crimean Astrophys. Obs.), DPV (P. Dubovsky), deM (E. de Miguel), IMi (I. Miller), Ioh (H. Itoh), KU (Kyoto U., campus obs.), Kaz (Kazan' Univ. Obs.), LCO (C. Littlefield), Mdy (Y. Maeda), RPc (R. Pickard), Shu (S. Shugarov team), Trt (T. Tordai).[§]The filter name C represents unfiltered observations.